Available online at www.sciencedirect.com
SCIENCE DIRECT®
Journal of Magnetic Resonance 170 (2004) 79–87
JMR Journal of Magnetic Resonance
www.elsevier.com/locate/jmr

Quantitative measurement of temperature by proton resonance frequency shift at low field: a general method to correct non-linear spatial and temporal phase deformations

S. Grimault, T. Lucas,* S. Quellec, and F. Mariette

Cemagref, Food Process Engineering Research Unit, 17 avenue de Cucillé, F-35044 Rennes Cedex, France

Received 27 January 2004; revised 22 April 2004
Available online 10 July 2004

Abstract

MRI thermometry methods are usually based on the temperature dependence of the proton resonance frequency. Unfortunately, these methods are very sensitive to the phase drift induced by the instability of the scanner which prevents any temperature mapping over long periods of time. A general method based on 3D spatial modelling of the phase drift as a function of time is presented. The MRI temperature measurements were validated on gel samples with uniform and constant temperature and with a linear temperature gradient. In the case of uniform temperature conditions, correction of the phase drift proved to be essential when long periods of acquisition were required, as bias could reach values of up to 200 °C in its absence. The temperature uncertainty measured by MRI was 1.2 °C in average over 290 min. This accuracy is coherent with the requirements for food applications especially when thermocouples are useless.

Keywords: MRI; Low-field scanner; Food; Phase shift; Thermometry

1. Introduction

Heat treatment is used in a large number of unit operations in the food industry, mainly for stabilization and preservation purposes. Heating, in the form of cooking, frying, or extrusion, also serves as a texturing process (e.g., crust formation). Heat treatment within food involves the development of a temperature gradient between the surface and the core [1] and applying uncontrolled heat treatment may jeopardize the overall food quality. Moreover, our knowledge of heat transfer within food is no longer appropriate in the ever-changing food market, which generates a range of foods varying greatly in composition and in geometry. Consequently, new advances in this field mainly rely on the development of temperature measurement techniques providing higher spatial resolution with good temporal resolution.

MRI thermometry is a non-invasive method very useful for studying food processing [2–6]. Among all the NMR parameters sensitive to temperature such as relaxation times T_1, T_2, diffusion coefficient, and chemical shift, the latter has been found to be the most efficient as it does not suffer from any physical structure dependency. In the case of stable scanner, and for a gradient echo sequence, local temperature can be inferred from the phase change $\delta\Phi$ between two MRI acquisitions separated by a time period of $\delta t = t - t_{\text{ref}}$ [7,8]:

$$T(t,x,y) = T_{\text{ref}} + \frac{\delta\Phi(x,y)}{\gamma\alpha B_0 \text{TE}}, \tag{1}$$

where B_0 is the main magnetic field, α is the proportionally constant (0.01 ppm/°C—[7,9]), γ is the gyromagnetic ratio of hydrogen, TE is the echo time of a gradient echo sequence. If there is now a phase drift due to scanner instability, the temperature calculation based on Eq. (1) will give erroneous results, as variations in

* Corresponding author. Fax: +02-23-48-21-15.
E-mail address: tiphaine.lucas@cemagref.fr (T. Lucas).

1090-7807/$ - see front matter © 2004 Elsevier Inc. All rights reserved.
doi:10.1016/j.jmr.2004.06.001

phase due to scanner instability will be wrongly attributed to temperature variation [10–12]. In such case, the chemical shift method requires either an extremely high stability of the magnetic characteristics of the scanner or short periods of use or at last, complementary developments to correct the drift generated by this instability. With this last objective, the contributions to the phase changes due to the temperature, $\delta\Phi_{\text{temperature}}$, and the scanner instability, $\delta\Phi_{\text{drift}}$, were assumed to be additive and the total phase change was given by [10]:

$$\delta\Phi_{\text{measured}} = \delta\Phi_{\text{drift}} + \delta\Phi_{\text{temperature}} \quad (2)$$

For evaluating $\delta\Phi_{\text{drift}}$, four isolated references with a constant and uniform known temperature were placed very close to the object under study. Then a linear spatial interpolation from these four local references allowed to estimate the phase drift at any position. Unfortunately because of the non-linear character of the deformation of the phase drift, this method did not prevent temperature error for acquisition times exceeding 1 h. Moreover, the use of a 1D linear model cannot be generalized to all MRI scanners. More recently, a variation correction algorithm has been proposed [13]. This elegant method suppressed the misalignment of the echo in the *K*-space which contributes significantly to the time-dependent background phase variations. The method evaluated at low field estimated temperature with an underestimation of −1.7 °C and a mean error of −0.8 °C. These results were valid over 1-h time frame for simulated thermal profile.

It should be pointed out that all the correction methods have been mainly developed for medical application purposes and specific methods are required for food application. For example, in medicine, a high temporal resolution is requested to monitor the temperature during the tissue destruction. For such application, the delay between the acquisition of the reference phase image and the consecutive phase image can be considered to be small compared to the time variation of the field inhomogeniety. Moreover, the temperature variation is mainly localized as hotspot and averaging from a region of interest (ROI) allows to increase the temperature accuracy. Heat treatments in food involve a large range of kinetics, from very fast temperature changes when using microwave or ohmic heating or frying to slower changes as those observed during refrigeration. Moreover, the temperature is spatially distributed over large distances and the temperature is directly measured from a single voxel without averaging. Therefore, a 2D or 3D correction methods of the temporal instability of *Bo* inhomogeneity is required and contrary to medical applications, this could be achieved with a thermally insulated reference phantom placed around the product. Since the temperature measurement are often performed over few hours, the stability of such correction should be assessed.

The main purpose of this paper is to propose a general method to correct errors in temperature mapping induced by non-linear phase drift. The method was applied to a low-field MRI scanner, which had strong drift over the measurement period. Dedicated experimental devices of broad usefulness have been developed for the validation of the method.

2. Materials and methods

2.1. Experimental device

The experimental device is schematically presented in Fig. 1. The *x*- and *y*-axes refer, respectively, to the horizontal and the vertical positions in the 2D image, while the *z*-axis refers to the image depth. The central part of the device, built of high density polyethylene, contained a gel ($100 \times 30 \times 50$ mm) which constituted the object under study. Four of its faces were well insulated (with high density polystyrene) so that only 1D heat transfer was possible, through the other two faces. Proper positioning of the object under study (and the whole experimental device) in relation to the antenna ensured that the direction of heat transfer was superimposed on the *y*-axis in the MRI image. At these gel surfaces, temperature was controlled by circulating a heating or a cooling water (cryostat Ministat, Huber, Germany), doped with 13.65 mmol/L of $MnCl_2$ to avoid motion artefacts in the images, and with an antifreeze agent (monoethylen-glycol) for low temperatures. The temperature reference object was a Plexiglas ring filled with the same gel as the central part of the device. A temperature-controlled (T_{ref}) liquid (doped water) was circulated on its four faces.

2.2. Gel preparation

Distilled water (351.96 g) with 47.96 g of low-low heat milk powder (INRA, Rennes, France) was stirred at ambient temperature. The addition of 12 g of glucono-δ-lactone (Sigma–Aldrich Chemie, Steinheim, Germany) induced a gradual decrease of the pH and then the formation of a gel. MRI measurements were delayed until the pH stabilized (at 3.9 after 16 h).

2.3. Thermocouple measurements

The two objects of the experimental device could be equipped with previously calibrated thermocouples (T-type, 0.2 mm diameter, kapton-insulated). Temperatures were recorded at 1-min intervals with a data logger (Hewlett–Packard 34970A). The temperature uncertainty was better than 0.5 °C. A preliminary study showed the absence in the temperature reference object of any temperature gradient within the gel and of any time deviation: $T(x, y, t) = T_{\text{ref}}$. During this work, T_{ref} was set at 25.4 °C. Thermocouples were introduced into

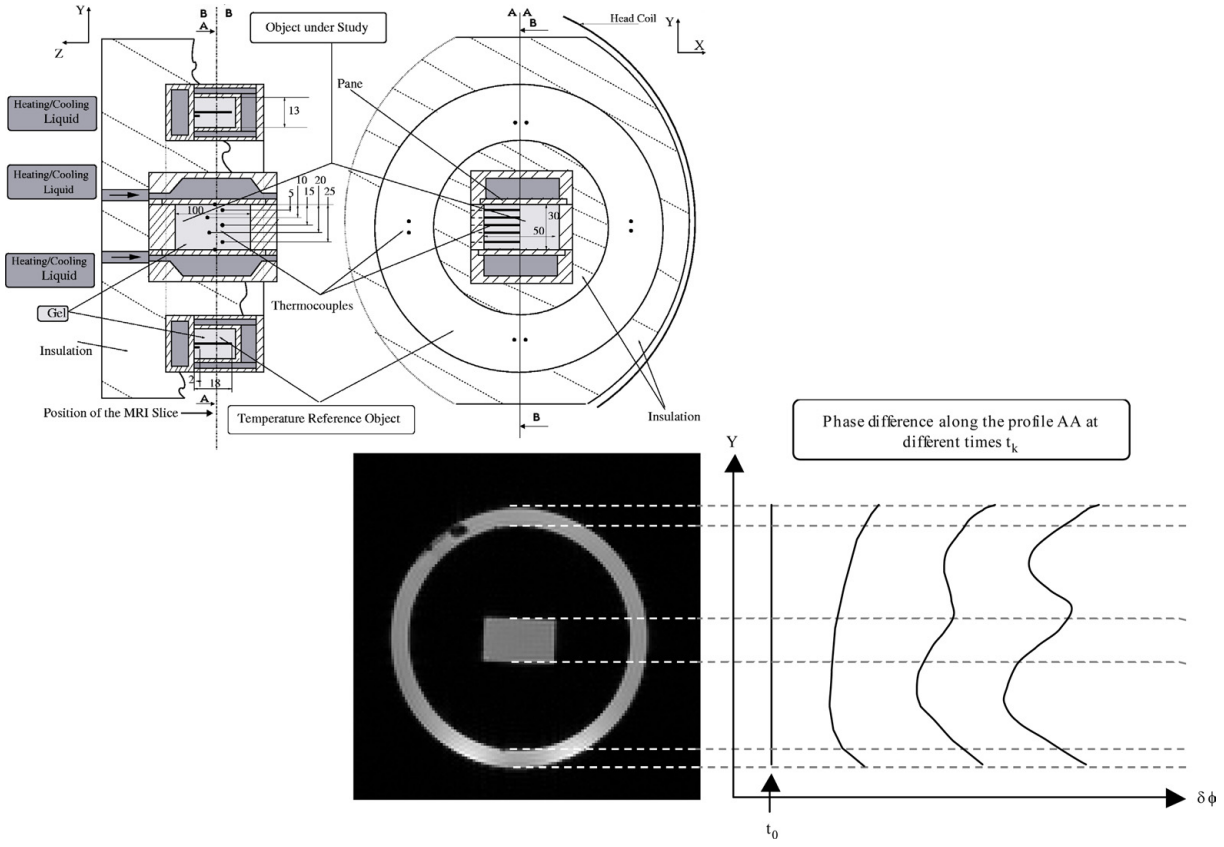

Fig. 1. Schematic representation of the experimental device made of two objects and of the deformations due to scanner instability observed on a phase difference image. Upper part: sagital (y, z plane) and transversal (x, y plane) slices of the experimental device. Lower part: MR amplitude image of the transversal slice of the device (at left) and possible time-course changes in the phase drift observed from the A–A′ profile (at right).

the central chamber perpendicularly to the heat transport flux and positioned every 5 mm along the y-axis (Fig. 1); they were placed in alternate rows along the z-axis to minimize disturbances of the heat transfer flow (± 8 mm from the A–A′ symmetry axis).

2.4. MRI experiments and signal analysis

MRI experiments were conducted using a clinical 0.2 T, electromagnet scanner (Magnetom Open, Siemens, Erlangen, Germany) fitted with a standard head coil. Phase images were acquired with a RF spoiled gradient echo sequence using the parameters TR = 150 ms, TE = 30 ms, FlipAngle = 40, matrix size = 128×128, FOV = 250×250 mm, slice thickness = 5 mm, and number of scans = 8. The voxel size was thus $1.87 \times 1.87 \times 5$ mm. The corresponding acquisition time was 2 min 36 s. Homemade algorithms were developed to build phase images directly from the raw data and to correct the original phase image for the phase wrapping [14]. The two objects were first segmented from the image background, thanks to a simple thresholding method applied on the MR amplitude image, and then separated using a labelling method. The phase difference images were obtained by voxel by voxel subtraction of the phase value in the image at a given time t from that in the reference phase image (acquired at t_{ref}). The phase difference in the temperature reference object was fitted with a 3D equation, using the Gnu Plot software (Free Software Foundation, Boston, USA) and a minimization procedure of the mean square differences. The phase difference in the object under study was then corrected for phase drift using the model equation previously adjusted on data from the temperature reference object—Eq. (2). At last, the corrected phase difference image was converted into a temperature map using Eq. (1). It should be stated that when applying Eq. (1), temperature dependent susceptibility effects could be neglected as a low field magnet was used and no thermal expansion occurred within the temperature range considered. Moreover, changes in the electrical conductivity of the gel were assumed to be negligible [15].

2.5. Validation procedure and data analysis

The present method was progressively validated in three steps.

First the extent of the phase drift, as well as the time-course evolution of its spatial distribution was assessed experimentally. The possibility of modelling the entire deformation surface using a reduced number of data

acquired at the extreme frontiers of the system under study will be validated experimentally.

Second, temperature was estimated in an object of uniform temperature. Although unrealistic for any application, this case study is advantageous for the validation process. The position to which the measurement is attributed is always accompanied with uncertainty. In the case of uniform temperature, the comparison between MRI and thermocouple measurements is facilitated by the freedom from positioning and any deviation between the two measurements (δ) can be fully attributed to the imperfections in the spatial modelling of the phase drift:

$$\delta = \overline{T}_{\text{mri}} - \overline{T}_{\text{thcpl}}, \tag{3}$$

$$SD_{\text{mri}} = \sqrt{\frac{\sum_{i=1}^{N}\left(T^i_{\text{mri}} - \overline{T}_{\text{mri}}\right)^2}{N-1}}, \tag{4}$$

where $\overline{T}_{\text{thcpl}}$ is the mean temperature calculated from the five thermocouples placed in the object under study, and $\overline{T}_{\text{mri}}$ is the mean temperature and its standard error (SD_{mri}), calculated from the temperature in the N voxels of a ROI, equivalent of the MRI gel image minus one row on each side along the y-axis and six columns on each side along the x-axis.

Third, temperature was estimated in an object presenting spatially varying temperature. So to minimize the number or the effect of different possible sources of bias, particular attention was paid to the estimation of position and a temperature gradient independent of time was preferred (no averaging over time). A sheet of plate of which parallel boundaries have constant but different temperatures, will develop a linear temperature gradient under stationary conditions [16]. In fact any temperature gradient encountered in processed foods can be approximated by adjacent linear segments of varying slopes and the whole range of slope values can be reproduced with the present device. A single MRI profile positioned in the area delimited by the two rows of thermocouples (Fig. 1) was extracted from the MRI temperature map. The freedom from bias of the MRI temperature was estimated by calculating the mean square difference (MSD_{mri}) between the temperature in each voxel i from the MRI profile and the thermocouple temperature estimated at the same position, after a linear regression has been performed:

$$MSD_{\text{mri}} = \sqrt{\frac{\sum_{i=1}^{N}\left(T^i_{\text{mri}} - T^i_{\text{thcpl}}\right)^2}{N-1}}. \tag{5}$$

3. Results and discussion

3.1. Characterization of the phase drift

This section characterizes the effect of the phase drift on the phase values and assesses the feasibility of modelling it. The temperature in the two objects was kept constant with time. Under this condition, only the phase drift can contribute to phase changes in the MR image. For simplicity of data analysis, a uniform temperature of 25.4 °C was set.

Major deformations between the surface and the core of the system were observed in the MR phase image (Fig. 2). Moreover, they were not constant in time. The surface generated by the phase drift was too complex for it to be modelled. However, modelling was possible when working on phase difference images (Figs. 3 and 4) calculated with reference to the image at t_{ref}. The new profile obtained at t_0 was then flat (Fig. 4). For $t > t_{\text{ref}}$, the profiles had a non-linear behavior with smoother spatial variations compared to the previous profiles extracted from the phase images (Fig. 4). Modelling of the surface could therefore be attempted. Numerous equations were tested and the best model was determined on the basis of the correlation coefficient (R^2). Whatever the time of acquisition, a polynomial equation of the second order with x and of the third order with y exhibiting a R^2 of over 0.99 was selected:

$$\delta\Phi_{\text{drift}} = ax + bx^2 + cy + dy^2 + ey^3 + f, \tag{6}$$

where x and y are the horizontal and vertical positions in the 2D image. It also presented fewer degrees of freedom than other polynomial equations (e.g., 5th order with x and y) and was therefore more robust to adapt to the time-course evolution of the phase drift.

The same approach, omitting the voxels from the object under study, was used when fitting. Whatever the acquisition time, the same equation as previously could also be selected ($R^2 > 0.99$). Small differences between the data generated by the models with or without the voxels from the object under study were observed. This is illustrated in Fig. 4 on vertical profiles at three different acquisition times. This was validated for any position of the profile in the image containing both objects. The differences in radians and converted into degrees Celsius observed in the object

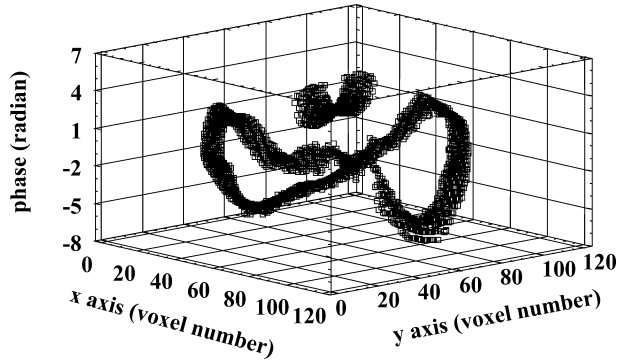

Fig. 2. Phase images at 25.4 °C showing the phase drift 2 h 15 min after acquisition of the reference image.

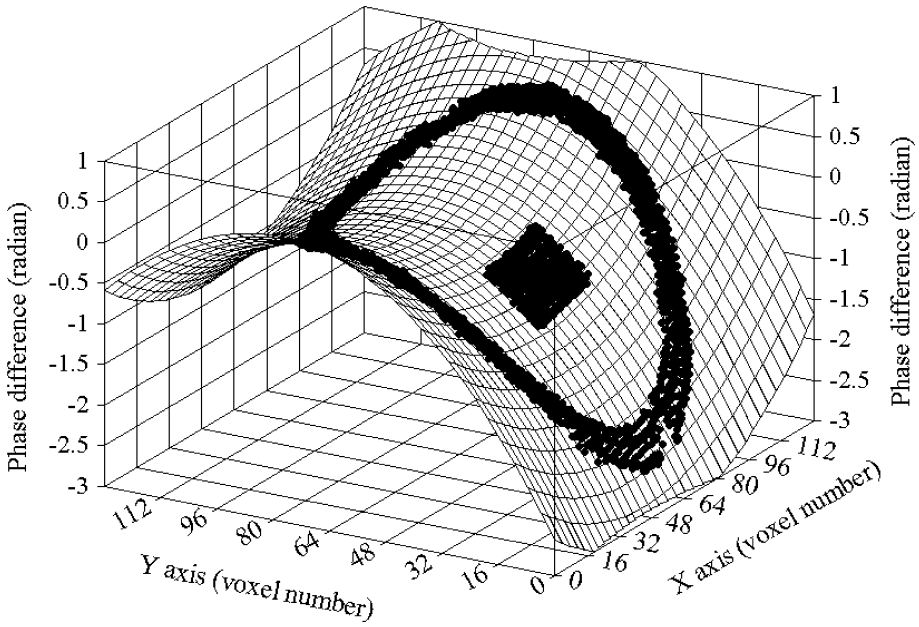

Fig. 3. Phase difference images at 25.4 °C showing the phase drift 2 h 15 min after acquisition of the reference image. MRI data (●) and data calculated from the model (dashed line) are presented.

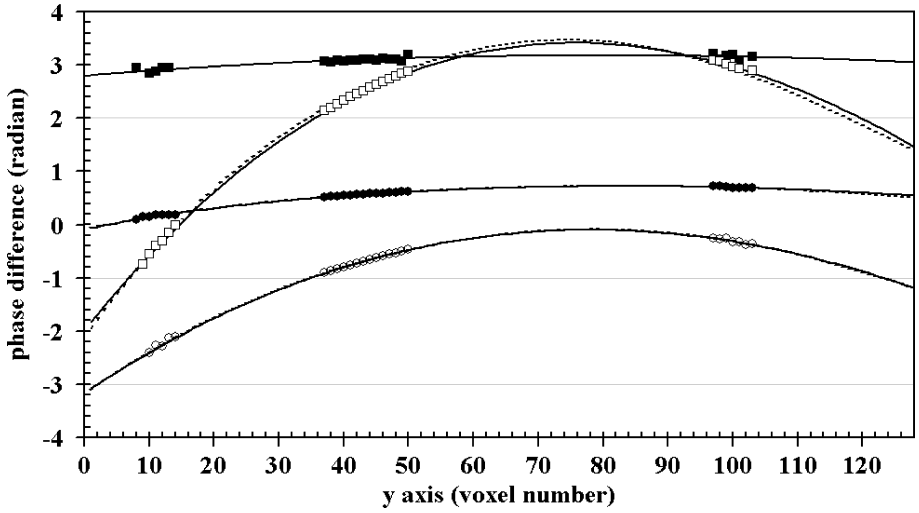

Fig. 4. Vertical profiles extracted from the MR phase difference images (64th column) acquired at 25.4 °C, 15 min (■), 30 min (●), 2 h 15 min (○), and 4 h 45 min (□) after acquisition of the reference image. Comparison with the data calculated from the model fitted with (dashed line) or without (plain line) the data from the object under study.

under study are given in Table 1. The difference in °C was small, 1.7 °C on average, with a minimum of 0.4 °C and a maximum of 3.3 °C. These results will be further discussed in the next section. Lastly, it is worth noting that if no correction was made for phase drift, the difference would vary between −10 and 200 °C depending on the extent of the local phase deformation.

All this demonstrated the feasibility of modelling the whole phase drift surface using only the behaviour of the voxels from the temperature reference object.

3.2. Validation of the method under different uniform and constant temperature conditions

The same approach was used at three different temperatures: 4.6, 25.4, and 40.0 °C (Table 1). The bias between the phase difference values measured by MRI in the object under study and the difference deduced from the model adjusted on the temperature reference object data alone was small. The average bias was 2, 2.7, and 3.3% for 4.6, 25.4, and 40 °C, respectively. It is

Table 1
Phase difference between experimental and calculated data expressed in radians and converted into °C for uniform and constant temperature conditions in the "object under study": (a) 4.6 °C, (b) 25.4 °C, and (c) 40.0 °C (temperatures controlled using thermocouples)

Time (min)	Phase difference between experimental and calculated data in the object under study (rad)	Standard deviation (rad)	Mean temperature calculated from MRI phase data (°C)	Temperature difference between MRI and thermocouple data (°C)	Standard deviation on MRI temperature (°C)
(a)					
30	6.36E−03	1.64E−02	5.0	0.4	1.0
60	3.65E−03	1.39E−02	4.8	0.2	0.9
90	3.65E−02	2.17E−02	6.8	2.2	1.4
120	2.93E−02	1.36E−02	6.4	1.8	0.8
150	2.73E−02	1.80E−02	6.3	1.7	1.1
180	5.24E−03	1.71E−02	4.9	0.3	1.1
210	2.61E−02	1.92E−02	6.2	1.6	1.2
(b)					
15	−2.43E−02	2.39E+01	24.1	−1.3	1.8
30	−2.73E−02	2.37E+01	24.3	−1.1	1.0
75	−2.27E−02	2.40E+01	25.0	−0.4	1.1
105	−4.22E−02	2.28E+01	24.4	−1.0	1.5
135	−4.78E−02	2.24E+01	23.5	−1.9	1.3
165	−5.28E−02	2.21E+01	23.4	−2.0	1.2
225	−8.11E−02	2.03E+01	22.8	−2.6	1.0
285	−8.23E−02	2.03E+01	22.1	−3.3	1.1
(c)					
60	2.43E−02	2.12E−02	41.5	1.5	1.3
90	2.25E−02	2.09E−02	41.4	1.4	1.3
120	1.30E−02	1.99E−02	40.8	0.8	1.2
150	2.20E−02	2.33E−02	41.4	1.4	1.4
180	6.20E−02	2.07E−02	41.2	1.2	1.3
210	4.96E−02	2.34E−02	43.1	3.1	1.5
240	4.14E−02	2.50E−02	42.6	2.6	1.6
270	3.01E−02	2.13E−02	41.9	1.9	1.3

The MRI data presented are the average and its standard deviation calculated over a region of interest (ROI) in the "object under study" (see Section 2).

worth remembering that in the actual configuration, the phase drift was the only source of changes in phase. If their spatial modelling were perfect, an absence of bias would be expected between MRI-calculated temperature and thermocouple temperature. The misadjustment of the phase drift induced an error in the temperature calculation. However, this error was also small, 1.7 °C on average, with a minimum of 0.2 °C and a maximum of 3.3 °C (Table 1 and Fig. 5). For specific sets of data, e.g., at 25.4 °C, the bias tended to increase

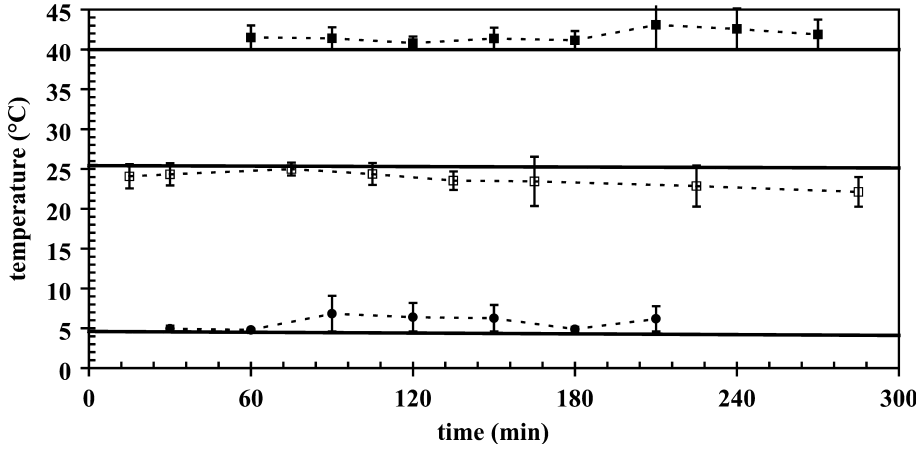

Fig. 5. Evolution with time of temperature measured by MRI (dashed line) and comparison with thermocouple measurements (plain line). The MRI data presented are the average and its standard deviation calculated over a region of interest (ROI) in the object under study under uniform and constant temperature conditions at 4.6 (●), 25.4 (□), and 40.0 °C (■).

as a function of the delay after the reference acquisition.

The error was of the same order of magnitude as the one reported in previous studies on high field scanners, which have a more stable and more homogeneous magnetic field. For example, the root-mean-square error measured on a 1.5 T scanner was less than 0.2 °C during the first hour but increased linearly despite correction of the phase drift and reached 1 °C after 4 h of acquisition [10]. All these results demonstrated that the 3D model used for the interpolation of the phase drift from the MRI data in the temperature reference object was efficient and gave a temperature measurement as good as the one obtained with higher field MRI scanners, whatever the temperature level when prolonged measurement periods are considered.

It was judged that the precision of the MRI temperature measurements was representative of the deviation of the MRI-calculated temperature calculated on a whole ROI. The standard deviation includes both the contribution of the signal-to-noise ratio and the spatial imperfections of the model used for the fitting of the phase drift. The standard deviation was small (1.2 °C on average) although the ROI in the object under study covered an extended spatial domain. This conclusion was independent of the temperature level in the object under study within the temperature range considered (4.6–40.0 °C). The standard deviation was also constant over several hours of measurement (Table 1 and Fig. 5). The levels of precision obtained in our studies were comparable to those previously reported for a 0.2 T scanner (± 1 °C) used in a 20-min experiment [11]. However, for a longer experiment [11], the accuracy increased to ± 2.5 °C whereas the one measured in our experiment stayed constant. The effect of the signal-to-noise ratio on accuracy could probably be improved by altering the MRI acquisition parameters: number of acquisitions, bandwidth, slice thickness, etc. For instance, the voxel volume in the present study (17.6 mm^3) was low compared to those used in previous studies, ranging from 26.9 mm^3 [10] to 54.93 mm^3 [11].

3.3. Validation of the method using an object with a linear temperature gradient

The objective of this last step was to estimate the pertinence of the present method in the case of significant variations in temperature between one voxel and the next.

Temperatures of the gel surfaces were set at 4 and 40 °C which produced a moderate slope value of 1.20 °C/mm (or 2.25 °C variation between two adjacent voxels). It should be remembered that to calculate the phase difference image, the temperature values at the reference time must be known. For this purpose, the temperature had previously been set at 25.4 °C in both objects. The reference phase image and the phase image acquired from the object under study when it had a stabilized linear temperature gradient were separated by 80 min ($t_{eq} - t_{ref}$). Thermal equilibrium (t_{eq}) was defined as the time necessary to observe a temperature variation of under 0.01 °C/s (time scale of 20 min) (see Fig. 6).

Temperatures acquired with thermocouples and those obtained from phase images are compared in stationary conditions ($t > t_{eq}$) in Fig. 6. The MRI temperature profile exhibited linear behavior, as expected. However, a significant bias between MRI and thermocouple values

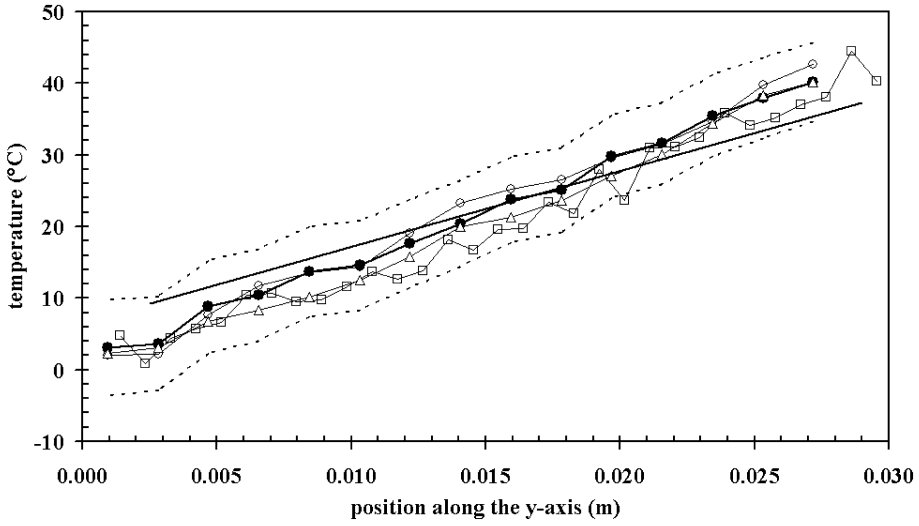

Fig. 6. Comparison of the linear temperature profile along the y-axis measured by MRI and by thermocouples (plain line). The temperature in the heat exchanger was set to 4.0 and 40.0 °C. The MRI temperature profiles were acquired 3 h 30 min (●), 4 h 30 min (○), and 6 h 00 min (■) after acquisition of the reference image using a 128 × 128 matrix, and 3 h 30 min (□) after acquisition of the reference image using a 256 × 256 matrix. The MRI profile at 3h30 is accompanied by its confidence interval (dotted line).

was observed ($MSD_{mri} = 3.40\,°C$). This value is slightly higher than the one observed under uniform and constant temperature conditions. According to Eq. (2), such a temperature bias could be attributed to either the signal-to-noise ratio of the phase difference image or the bias generated by the modelling of the phase drift. Both sources of deviation are discussed below.

The bias between thermocouple and MRI data was not affected by the averaging of up to 9 MRI profiles (the area under consideration is then the same as that covered by the thermocouples). In fact, temperature along a row (x-axis) could be considered to be constant (± 0.5–$1.4\,°C$ depending on the temperature level). Additionally, the bias was not affected by either the acquisition number or the higher resolution (256×256) (Fig. 6). This meant that the source of the bias could not be attributed to the noise in the image but to the imperfections in the modelling. Evidence of this is the absence of statistical difference between the MRI temperature and the thermocouple temperature when the MRI profile was accompanied by its 95% confidence interval ($\pm 6\,°C$ on average) (Fig. 6).

The degradation of the modeling in the case of linear temperature gradient with reference to uniform temperature conditions was explained by the slight displacement of the object under study to areas of maximum phase deformation—which can be predicted with lesser confidence than in the case of uniform temperature conditions. This result illustrates the importance of the position of the object under study relative to the phase deformations and the accuracy of the interpolation of the phase drift. The strategy to reduce the confidence interval relies on moving the object under study to areas of smaller phase deformation or adapting the design of the temperature reference object to improve the accuracy of the modelling of the phase shift. In the latter case, a first approach would be to decrease the distance between the temperature reference object and the object under study. However, such a solution would imply a finer control of heat exchanges within the device.

4. Conclusion

The results can be considered excellent, remembering that the objective of predicting the phase drift was challenging. The first difficulty concerned the continuity of the phase drift phenomena (in space and time). The second difficulty was the feasibility of modelling these changes solely by fitting the behavior of selected voxels located close to the antenna. Thanks to pre-correction of the phase difference values, the MRI temperature values were close to the values obtained with a thermocouple under uniform and constant temperature conditions, differing by under $2\,°C$. Moreover, the time stability was significantly improved. The bias observed in the case of a linear temperature gradient must not be considered as a final criterion of evaluation of the present method, since the position of the object was not optimal.

The present method could be further improved. Optimizing the number and the location of the voxels used for the modelling, and filtering the data could both improve the performance of the model. Improving the signal-to-noise ratio by optimizing the acquisition parameters would undoubtedly give better accuracy. The effect of increasing the TE to increase the temperature sensitivity according to the echo-shifted flash sequence could also be evaluated [11]. The MRI method could also be further evaluated for other temperature gradient conditions. It is worth underlying the experimental device makes it possible to increase the slope value by increasing the difference between the temperatures of each boundary or reducing the thickness of the sheet.

The uncertainty of the present MRI method is obviously higher than the one obtained by thermocouples ($\pm 0.5\,°C$ on average). However, the spatially rich character of the MRI method may balance the degradation of the temperature uncertainty. First in the case of MRI, the position attributed to the temperature data are known with a better accuracy. Second, the use of thermocouples fails to assess the spatial distribution of temperature in foods of complex geometry or placed in a complex thermal environment and especially to characterize the out-coming "hot spots" and "cold spots" which may be source of either over cooking or imperfect microbial inactivation. Additionally, some fragile food products do not allow invasive measurements. In all these cases, accessing non-invasively the spatial distribution of temperature although with higher level of uncertainty will be preferred.

References

[1] R. Toledo, Fundamentals of Food Process Engineering, Van Nostrand Reinhold, New York, 1991.
[2] B. Hills, Magnetic Resonance Imaging in Food Science, Wiley-Interscience, New York, 1998.
[3] R.R. Ruan, P.L. Chen, Water in Foods and Biological Materials. A Nuclear Magnetic Resonance Approach, Technomic Publishing, Lancaster, 1998.
[4] M.D. Mantle, A.J. Sederman, Dynamic MRI in chemical process and reaction engineering, Prog. Nucl. Mag. Res. Spectrosc. 43 (2003) 3–60.
[5] L.D. Hall, M.H.G. Amin, S. Evans, K.P. Nott, L. Sun, Magnetic resonance imaging for industrial process tomography, J. Electron. Imaging 10 (2001) 601–607.
[6] K.P. Nott, L.D. Hall, J.R. Bows, M. Hale, M.L. Patrick, MRI mapping of temperature distribution induced in food by microwave heating, Magn. Reson. Imaging 18 (2000) 69–79.
[7] J.C. Hindman, Proton resonance shift of water in the gas and liquid states, J. Chem. Phys. 44 (1966) 4582–4592.

[8] Y. Ishihara, A. Calderon, H. Watanabe, K. Mori, K. Okamoto, Y. Suzuki, K. Sato, K. Kuroda, N. Nakagawa, A. Tsutsumi, A non-invasive temperature mapping using water proton chemical shift, in: Proceedings of SMRM 11th annual Scientific Meeting, Berlin, 1992, p. 4803.
[9] X.F. Ye, R. Ruan, P. Chen, K.H. Chang, K. Ning, I.A. Taub, C. Doona, Accurate and fast temperature mapping during ohmic heating using proton resonance frequency shift MRI thermometry, J. Food Eng. 59 (2003) 143–150.
[10] J. DePoorter, C. DeWagner, Y. DeDeene, C. Thomsen, F. Stahlberg, E. Achten, The proton resonance frequency shift method compared with molecular diffusion for quantitative measurement of two dimensional time dependent temperature distribution in a phantom, J. Magn. Reson. 103 (1994) 234–241.
[11] Y.C. Chung, J.L. Duerk, A. Shankaranarayanan, M. Hampke, E.M. Merkle, J.S. Lewin, Temperature measurement using echo-shifted FLASH at low field for interventional MRI, J. Magn. Reson. Imaging 9 (1999) 138–145.
[12] Y. Ishihara, A. Calderon, H. Watanabe, K. Okamoto, Y. Suzuki, K. Kuroda, A precise and fast temperature mapping using water proton chemical shift, Magn. Reson. Med. 34 (1995) 184–823.
[13] K.J. Barkauskas, J.S. Lewin, J.L. Duerk, Variation correction algorithm: analysis of phase suppression and thermal profile fidelity for proton frequency magnetic resonance thermometry at 0.2 T, J. Magn. Reson. Imaging 17 (2003) 227–240.
[14] M. Desvignes, S. Langlois, J.M. Constans, M. Revenu, Déroulement de phase: applicationàla correction de distorsions géométriques en IRM, Traitement du Signal 17 (2000) 313–324.
[15] R.D. Peters, R.M. Henkelman, Proton-resonance frequency shift MR thermometry is affected by changes in the electrical conductivity of tissue, Magn. Reson. Med. 43 (2000) 62–71.
[16] H.S. Carslaw, J.C. Jaeger, Conduction of Heat in Solids, Clarendon Press, Oxford, 1959.